Load testing of a deteriorated prestressed concrete girder bridge without plans

Castellanos-Toro, Sebastián ; Millán, Diana ; Ortiz, Albert R. ; Marulanda, Johannio ; Thomson, Peter ; Lantsoght, E.O.L.

Publication date
2022

Document Version
Final published version

Published in
ACI Special Publication

Citation (APA)
Castellanos-Toro, S., Millán, D., Ortiz, A. R., Marulanda, J., Thomson, P., & Lantsoght, E. O. L. (2022). Load testing of a deteriorated prestressed concrete girder bridge without plans. *ACI Special Publication*, *352*, 16-35.
https://www.concrete.org/publications/internationalconcreteabstractsportal.aspx?m=details&id=51734854

Load testing of a deteriorated prestressed concrete girder bridge without plans

Sebastián Castellanos-Toro, Diana Millán, Albert R. Ortiz, Johannio Marulanda,
Peter Thomson, Eva O.L. Lantsoght

Synopsis: In this study, a prestressed concrete girder bridge without plans and with severe levels of deterioration, located in Cali, Colombia, was load-tested to quantify, experimentally, its live-load behavior. The bridge consists of seven prestressed I-girders covered with a reinforced concrete deck, and four diaphragm beams. A geometric survey was performed to obtain the dimensions for a shell-based linear finite-element model (FEM) representing the bridge superstructure. In this survey, it was observed that the diaphragm beams in the span are geometrically inadequate to contribute to the structural system. Based on the experimental modal properties and the design regulations enforced at the time of bridge design and construction, a first update was made. Modifying the effective stiffness of selected elements to model girder deterioration, a second update was performed based on strain-gauge data from three load tests and visual inspection (VI) of the elements. The three models (basic, modal updated, and load-test/VI updated) were compared with the load distribution factor (DF) obtained from the load test and AASHTO distribution factor estimations. Visual inspection, dynamic characterization, and load testing response of this structure indicated severe deterioration of the girders and the absence of the effect of the diaphragms in the overall structural behavior. The results show that the AASHTO recommendations overestimate the LDF in comparison with the FEM without girder deterioration. When girder deterioration is included in the model, the LDFs change drastically, showing that AASHTO estimations are not in line with the experimental results. As such, for cases of bridges with severe levels of deterioration, it is recommended to use field data to estimate the distribution factors.

Keywords: dynamic characterization, load distribution factors, load testing, prestressed concrete girder bridge, strain measurement, visual inspection.

INTRODUCTION

The decision-making on maintenance, repair, reconstruction, or replacement of a structure such as a bridge must be based on the evaluation of its safety and load capacity using reliable criteria such as geometric details, material properties, reinforcement configurations, inspection reports and even prior load rating files[1]. The assessment process (structural performance or load capacity quantification) starts from an analytical inference based on the structural design of the bridge to predict the behavior of the in-service structure. However, for bridges in operation, information like the design or as-built plans may be limited or non-existent[2]. Besides, the analytical inference of the load effect (load distribution and load paths) and the structural capacity of the in-service structure can be affected because of deterioration and the level of damage on the structural elements, which generates and increases the uncertainty on the behavior evaluation and load rating quantification of the bridge[3,4].

For the design of a new bridge or evaluation of an existing one, distribution factors for transverse distribution of live loads can be used. This phenomenon is typically defined using prescriptive formulas that simplify the complex behavior into simple factors. In the Americas, the common practice is to use the formulation proposed in AASTHO standards[5,6], whereas in Europe the Guyon-Massonet method is more commonly used[7]. In recent decades, several methods such as finite element modeling (FEM) and load testing have become accepted methods for determining live load distribution[8]. Some investigations show that distribution factors calculated using AASHTO standards give more conservative and even poor estimations when compared with distribution factors generated with the FEM and experimental approaches[9,10,11].

Load testing of bridges is a method that allows the assessment of bridge performance, especially when analytical methods do not provide accurate answers about the bridge's behavior[12]. Information about bridge load testing and experimental live load distribution factor determination can be found in the literature. The ACI 342R-16 Report[8] provides basic guidance on the methods and tools available for determining flexural live load distribution behavior of in-service concrete bridges. Studies such as those carried out by Lantsoght et al.[4] and Halicka et al.[13] show the development of load tests during the last two decades, where the following is highlighted: (1) the existing types of load tests according to the load to be applied or the objective of the test, (2) the criteria for the application of the test, such as the maximum load to be applied or the objective test load and the criteria to stop the test in progress, (3) the protocols established in international standards for the application of load tests on bridges, and (4) the existing codes and guides for the execution of load tests on concrete bridges. Recent research, such as the studies conducted by Ohanian et al.[9], Torres et al.[10], Dong et al.[11] and show the procedures applied to determine, experimentally, the live load distribution factors through load testing, including finite element model calibration based on experimental results and comparison with code specifications. The first work shows the benefits of performing an in-place load test creating calibrated models for two study cases, the results show that standard moment distribution factors calculated by AASHTO are, at least, two times higher than those predicted by a calibrated model. Finally, from the updated models, live load distribution factors can be used to calculate a more realistic load rating. The second study highlights a poor agreement between AASHTO LRFD Girder Distribution Factor (GDF) equations and FEM-estimated GDF for double tee bridges and proposes new equations based on a multivariable linear regression using a shell-based updated model. The last work shows that for a pre-stressed girder bridge the distribution factors of live load calculated by AASHTO standards gives more conservative results when compared with the experimental and FEM approaches. Thus, the load-rating factor (RF) of live load calculated by AASHTO standards gives more conservative results as well.

In this paper, a prestressed girder bridge without plans and severe levels of deterioration, located in Cali, Colombia, was load-tested to quantify, experimentally, its live-load behavior. The selection of this type of bridge (one span and its type of superstructure and construction materials) is based on an inventory of the bridges in the city from 2015. That study showed that 76% of the total vehicular bridges are one span and 42% of the total vehicular bridges are constructed of prestressed concrete beams. Since the bridge does not have plans or design information, and some construction flaws and severely deteriorated girders (bottom flanges and webs) were detected, different field data were collected. Data on the state and performance of the bridge was collected by means of a geometric survey with a visual inspection, acceleration records for dynamic characterization, static load testing with strain measurements. The goals of this research are as follows: (i) estimate the design live load of the super-structure, (ii) infer which elements contribute to the stiffness of the structural system, (iii) obtain the live load distribution of the bridge girders and explore if the behavior under live loads relates to the cracked cross-section, (iv) determine how different levels of experimental information contribute to improving the estimation of the bridge response, and (v) investigate if the observed damage is caused by live loads.

RESEARCH SIGNIFICANCE

The presented research combines field testing and finite model updating to represent the actual behavior of a planless, deteriorated prestressed concrete girder bridge. Being a structure without as-built or design plans and some level of deterioration, the steps described herein can be valuable to improve the current practice of service evaluation of this type of bridges and to contribute to the field of assessment of existing infrastructure assisted by field data. The research also shows that the AASHTO live load distribution factors cannot be used for the assessment of existing prestressed concrete girder bridges in which cracking is present.

BACKGROUND

In Colombia, the American Association of State Highway and Transportation Officials (AASHTO) specifications were used for bridge design until 1994. In 1995, the 1st Edition of the Colombian Bridge Seismic Design Code CCP-95[14] was published for the Colombian national institute of roads - INVIAS. This code was based on the AASTHO Standard Specification for Highway Bridges - 1992[15]. In 2013, the INVIAS and the Colombian Association of Seismic Engineering - AIS published a new edition of the Colombian Bridge Design Code called CCP-14[16]. The CCP-14 is based on AASHTO LRFD Bridge Design Specifications (6th and 7th editions)[17,18].

Wheel factors and live load distribution factors

The CCP-95[14] (AASTHO Standard-1992) specification states: as an approximate method of analysis, the determination of the bending moments due to live load on the longitudinal girders in the superstructure should be done based on the wheel load and the wheel factors (WF). For a concrete deck on prestressed girders, the wheel factors for interior girders are shown in Eqn. 1 for a bridge designed with one traffic lane loaded and Eqn. 2 for a bridge designed with two or more traffic lanes loaded.

$$WF = S/2.1 \text{ for } S \leq 3.0 \quad (1)$$

$$WF = S/1.7 \text{ for } S \leq 4.0 \quad (2)$$

where S is the distance in meters between adjacent girders. For the exterior beams, the code indicates that the live load distribution factor for bending moment shall be determined as the reaction of the wheel load obtained when assuming that the deck slab acts as a simple span between beams (lever rule). These distribution factors (CCP-95, AASTHO Standard 1992, 1996 and 2002) were based on a wheel line concept—or half of a truck load[8].

The CCP-14[16] is the current bridge design code in Colombia (AASHTO LRFD Specifications 6th and 7th). The live load distribution factors for bending moment are based on a lanes concept (whole truck load) and not a wheel line concept (half of a truck load). The load distribution factor equations in the AASHTO LRFD Specifications are empirical and differ greatly from the S-over method prescribed in the AASTHO Standard. The load distribution factor equations are grouped by bridge type and are generally functions of girder spacing (S), span length (L), slab thickness (t_s) and beam stiffness (K_g)[8]. For a concrete deck on a prestressed girder superstructure, the live load distribution factor (g) equations for interior girders for bridges designed for one traffic lane loaded or for two or more lanes loaded are shown in Eqn. 3 and Eqn. 4, respectively.

$$g = 0.06 + \left(\frac{S}{4300}\right)^{0.4} \left(\frac{S}{L}\right)^{0.3} \left(\frac{K_g}{Lt_s^3}\right)^{0.1} \quad (3)$$

$$g = 0.075 + \left(\frac{S}{2900}\right)^{0.6} \left(\frac{S}{L}\right)^{0.2} \left(\frac{K_g}{Lt_s^3}\right)^{0.1} \quad (4)$$

and

$$K_g = \frac{E_B}{E_D}\left(I + Ae_g^2\right) \quad (5)$$

where S, L and t_s are in mm, and K_g is mm^4. E_B is the modulus of elasticity of the beam material in MPa, E_D is the modulus of elasticity of the deck material in MPa, I is the moment of inertia of the noncomposite beam in mm^4, A is the area of the noncomposite girder in mm^2 and e_g is the distance between the centers of gravity of the basic beam and

deck in mm. The equations above have application ranges for the variables S, L, t_s and K_g[16,18]. S must be in the range of 1100 mm (43.34 in.) and 4900 mm (193.06 in.), L between 6000 mm (19.7 ft) and 73000 mm (239.68 ft), t_s between 110 mm (4.33 in.) and 300 mm (11.82), and K_g between 4.1623x10^9 mm^4 (1.00x10^4 in^4.) and 2.9136x10^{12} (7.02x10^6 in^4.).

For exterior girders, the live load distribution factors (g) can be calculated using the lever rule when one traffic lane is loaded. For two or more lanes loaded, g can be obtained by multiplying the interior girder load distribution factor ($g_{interior}$) by a correction factor (e), which is calculated using Eqn. 6.

$$e = 0.77 + \frac{d_e}{2800} \tag{6}$$

where d_e is the horizontal distance in mm from the centerline of the exterior web of the exterior girder at the deck level to the interior edge of the curb or traffic barrier[16,18].

Distribution factors calculated using experimental data and FEM results

The bridge load distribution can be obtained using the response across the bridge cross-section (displacements or strains). Based on displacement data, the girders distribution factor is obtained by dividing each girder displacement by the summation of all girders displacements[11]. Just as for the approach based on displacements, the strain-based method uses the ratio of the measured strain in an individual girder divided by the summation of the strains in all girders to determine the distribution factor (DF) as shown in Eqn. 7[8,19,20].

$$DF_i = \frac{n \cdot \varepsilon_i}{\sum_{j=1}^{k} \varepsilon_j \cdot w_j} \tag{7}$$

where ε_i is the strain at the i-th girder; w_i is the ratio of the section modulus of the i-th girder to the section modulus of a typical interior girder; n is the number of wheel lines of applied loading; and k is the number of girders.

BRIDGE DESCRIPTION

The bridge over the Lili River was constructed in the 2000s in the neighborhood Ciudad Jardin, south of Cali, Colombia. It consists of two lanes with the same traffic direction as shown in Fig. 1(a), a bike lane on the left side, and a pedestrian platform on the right side. This structure is a prestressed straight girder bridge with a 19 m (62 ft) span, a 12.2 m (40 ft) width, and with no intermediate supports. The concrete deck sits on seven prestressed I-beams and there are also four diaphragms, two near the supports and two positioned at one-third points of the span as shown in Fig. 1(b). The bridge was designed and constructed in the early 2000s when the 1st Edition of the Colombian Bridge Code CCP-95[14] was in effect (based on the AASTHO Standard Specification for Highway Bridges - 1992). The construction plans for the bridge were not obtainable; thus, information regarding wearing surface and deck thickness, design materials properties, bearings characteristics, passive and active reinforcement configuration, and element dimensions were not available.

Fig. 1—Overview of bridge tested: (a) traffic flow view; (b) bottom view.

A basic procedure to obtain the required information was developed. First, a geometry survey was completed to obtain the dimensions of the girders, diaphragms, and separations between them. Also, the lengths of the cantilevers where

the bike lane and the pedestrian platform are located were determined. The thickness of the deck and wearing surface together was obtained indirectly using the interior and exterior heights of the curb. Second, information regarding material properties (concrete and prestressing steel) and bearing elements was assumed from the Colombian bridge specification[14] enforced at the time of bridge design and construction. These properties were corroborated using construction plans from other bridges with similar characteristics that were designed and constructed at the same time as the bridge under study. Third, the prestressing force and eccentricity were estimated using Magnel diagrams[19]; the truck loadings and distribution factors (wheel factor) were based on the serviceability criteria established by the CCP-95 at that time. Finally, a visual inspection was performed at the same time as the geometric survey to observe the level of deterioration of the principal elements.

Geometric survey and visual inspection of the girders

The results of the geometric survey are shown in Fig. 2. The seven girders are 872 mm (34.3 in.) deep and have a bottom flange width of 454 mm (17.9 in.). The separation between adjacent beam is 1500 mm (59 in.) and the combined thickness of the wearing surface and concrete deck is 200 mm (7.9 in.). Based on CCP-95 recommendations, a minimum thickness of 160 mm (6.3 in.) for the concrete deck was assumed since it is conservative. Thus, the deck and wearing surface thickness are assumed as 160 mm (6.3 in.) and 40 mm (1.6 in.), respectively.

A visual inspection was performed to determine the level of deterioration of the girders. In this activity, the length, width, and location of the cracks at the girder surfaces were acquired. Fig. 3 shows the deterioration level in two elements, girders 1 and 2. In Fig. 3, the approximate length and measured width of a crack are presented in square and round brackets, respectively. Girder 2 is the most deteriorated element and girder 4 has a similar crack pattern to girder 2 (quantity and thickness). The other girders have a level of damage less than girder 1.

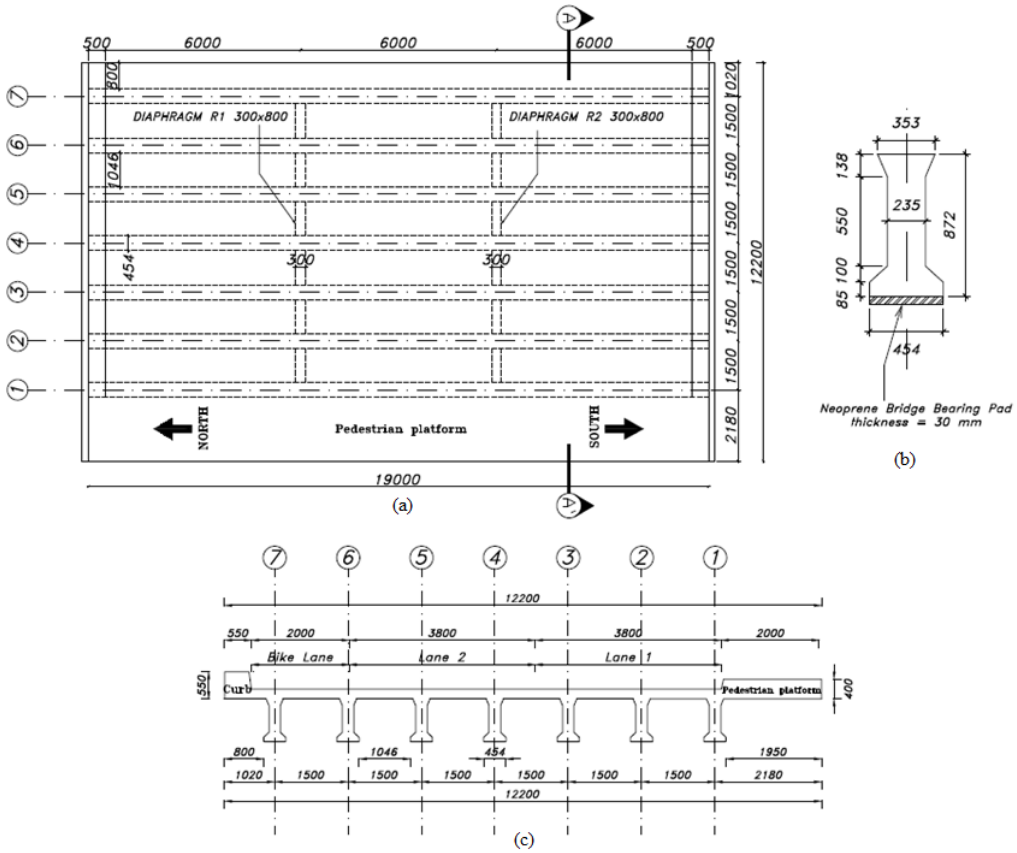

Fig. 2—Bridge geometry survey: (a) plan view; (b) beam detail; (c) cross-section view (section A-A'). Dimensions in mm [1 mm = 0.0394 in.]

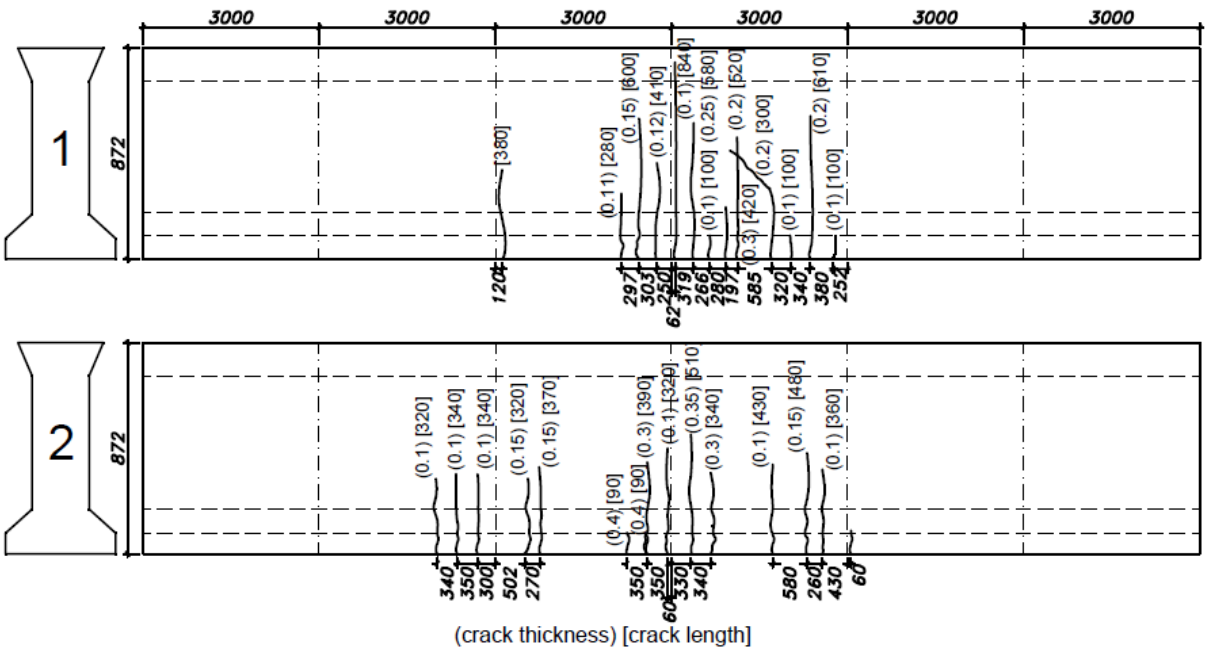

Fig. 3—Cracking determined through visual inspection for girders 1 (top) and 2 (bottom). Dimensions in mm [1 mm = 0.0394 in.]

ESTIMATE OF PRESTRESSING FORCE

Before load testing, the prestressing force and eccentricity were estimated using Magnel diagrams for the two design trucks from CCP-95[14]. Based on the serviceability criteria (i.e., allowable stresses) for compression and tension at transfer and service, the Magnel equations establish the range of solutions that satisfy the serviceability criteria at the beam midspan based on the bottom compressive stress at transfer (σ_{ci}), top tensile stress at transfer (σ_{ti}), bottom tensile stress at service (σ_t), and top compressive stress at service (σ_c). The Magnel diagram is constructed by plotting four lines based on four inequations[21]; two inequations that correspond to the beam stresses at transfer are not affected by the truck loading, the other inequations that satisfy the serviceability criteria are affected by the truck loading[2]. The area enclosed by the four lines, and the straight lines with the geometry limits based on the actual size of the girder, represents the possible combinations of the initial prestressing force (F_o) and eccentricity (e) satisfying the allowable stresses at transfer and service. For systems like the girder-slab bridges, it is important to verify if the allowable stresses in service are satisfied by the simple beam section or composite beam and deck cross-section.

Allowable stresses and design trucks from CCP-95

The bridge was designed and constructed in the early 2000s when the 1st Edition of the Colombian Bridge Code CCP-95[14] was in effect. Based on these specifications, the beam concrete strengths were assumed to be 28 MPa (4061 psi) at transfer (f'_{ci}) and 35 MPa (5076 psi) at service (f'_c). The prestressing steel was assumed to be 12.7 mm (0.5 in.) diameter, Grade 270, stress-relieved strand, and the prestress losses were estimated as 15%. The allowable stresses in Table 1 were taken from the CCP-95.

Table 1—Allowable stresses from CCP-95.

Allowable stress	Equation	Units	Value
Bottom compressive stress at transfer (σ_{ci})	$\sigma_{ci} = 0.55\, f'_{ci}$	MPa (psi)	15.40 (2234)
Top tensile stress at transfer (σ_{ti})	$\sigma_{ti} = 0.25\, (f'_{ci})^{1/2}$	MPa (psi)	1.32 (192)
Bottom tensile stress at service (σ_t)	$\sigma_t = 0.50\, (f'_c)^{1/2}$	MPa (psi)	2.96 (429)
Top compressive stress at service (σ_c)	$\sigma_c = 0.40\, f'_c$	MPa (psi)	14.00 (2031)

The design trucks specified in CCP-95 are named C40-95 and C32-95. The CCP-95 allows to use the lightest truck for the design of the bridge based on the function of the roadway where the bridge is located. Fig. 4 describes the axle weight of each truck. The Colombian specification states that, for bridges with spans less than 28.0 m (91.8 ft), the

design live load must be the truck load only (wheels lines concept – the axle weight divided by two) multiplied by the wheel factor (calculated with Eqn. 2) and the impact allowance (I) calculated with Eqn. 8:

$$I = \frac{16}{L_c+40} \quad (8)$$

where L_c is the distance between bearings in meters. The live load impact and wheel factor for an interior girder were computed as 1.28 and 0.88, respectively. The dead load moment was computed from the beam, deck, and wearing surface self-weights.

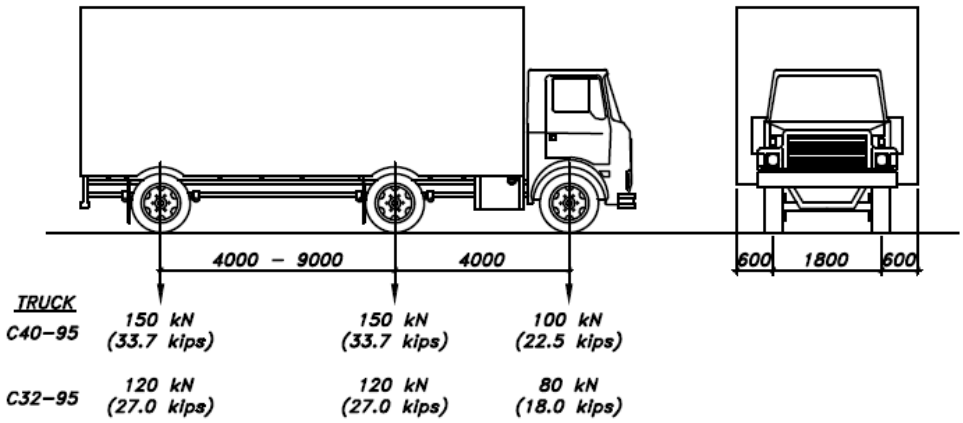

Fig. 4—Design trucks from CCP-95. Dimensions in mm [1 mm = 0.0394 in.]

Prestressing force estimation

Fig. 5 shows the Magnel diagram for the C32-95 design truck with the assumption of a composite section for the serviceability stage (Inequation III for top compressive stress at service (σ_c) and inequation IV for bottom tensile stress at service (σ_t)); at this stage, the simple section was discarded because it did not meet the allowable stress criteria presented in Table 1. Furthermore, the Magnel diagram using the C40-95 design truck doesn't show an area enclosed by the four lines, which indicates that the section (simple or composite) is insufficient for this load. Table 2 summarizes the assumed eccentricity based on the supposed cover and actual geometry (e_g), the high prestress (F_{omax}), low prestress (F_{omin}) and the effective force (F_e). F_{omax} and F_{omin} were obtained from Magnel diagram as the inverse values in the intersections of the straight line (eg) with line (II) and line (IV), respectively. As conservative criterion, F_e was computed as kF_{omin} with k equal to 0.85 (prestress losses of 15%), and the area of the prestressing strand (A_s) was obtained by dividing F_e by the initial strand stress at transfer (f_{so}), which was assumed to be the minimum of 74% of the ultimate strand stress (f_{pu}) or 82% of the yield strand stress (f_{py}) as specified in the CCP-95. Later, A_s and F_e were corrected with an integer number of strands as shown in Table 2.

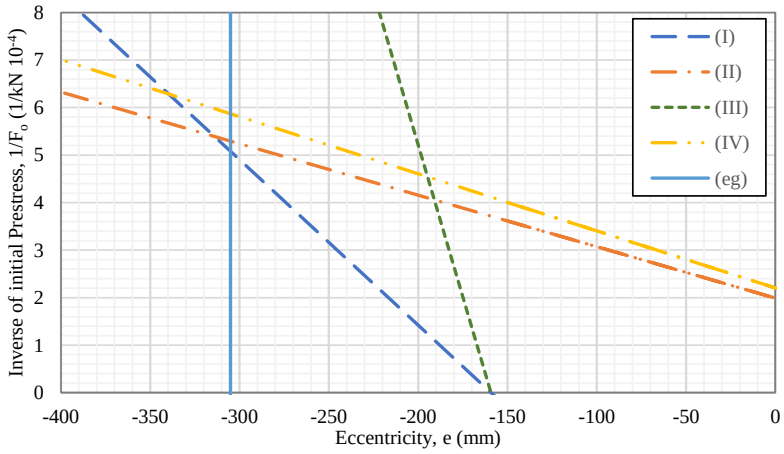

Fig. 5—Magnel diagram for C32-95 design truck. [1 kN = 0.2248 kip; 1 mm = 0.0394 in.]

Table 2—Estimate of prestressing force for the bridge.

Parameter	Units	Value
High prestress (F_{omax})	kN (kip)	1888.1 (424.4)
Low prestress (F_{omin})	kN (kip)	1704.3 (383.1)
Assumed eccentricity (e_g)	mm (in.)	305 (12)
Corrected effective force (F_e)	kN (kip)	1477 (332.0)
74% of the ultimate strand stress ($0.74f_{pu}$)	MPa (ksi)	1404.7 (203.6)
82% of the yield strand stress ($0.82f_{py}$)	MPa (ksi)	1354.2 (196.4)
Corrected area of the prestressing strand (A_s)	mm^2 (in^2)	1283 (1.99)
Number of strands	-	13

EXPERIMENTS

Operational modal analysis

An operational modal analysis (OMA) was performed to identify the dynamic properties of the bridge through ambient vibration tests. The ambient vibration records are produced by vehicles and pedestrians, the wind flow, and micro-tremors in the area. The vibration tests were carried out during the normal operation of the bridge without interrupting traffic. The acceleration records were taken at 18 points in vertical and transverse directions: six on the curb, six on lane 1, and six on the pedestrian platform. The equipment used for this work was composed of six accelerometers, three of which were a REF-TEK model 130-SMA triaxial instrument and three of which were uniaxial REF-TEK model 131B-01/1 accelerometers. All accelerometers had an acceleration range of ± 4g. The obtained signals are converted from analog to digital with a 24-bit card incorporated in the equipment.

With this modal information, a first update of the bridge finite element model was performed. Fig. 6(a) shows the acceleration time histories of one configuration over the deck at different points along girder 3 using the six-channel equipment as a typical register of operational vibration. Fig. 6(b) shows the power spectral density analysis (PSD) of acceleration at the same register to identify possible modal frequencies. Using all the collected vibration records, three operational modal analysis methods were employed to identify the modal frequencies, damping ratio and mode shapes, including: (1) peak-amplitude or peak-picking (PP) with transmissibility between outputs[22], (2) the natural excitation technique with eigensystem realization algorithm (NExT-ERA)[23], and (3) data-driven stochastic subspace identification (DD-SSI)[24]. For the NExT-ERA and DD-SSI methods, a stabilization process was performed for grouping similar frequencies and eliminating spurious modes[25]. Fig. 7 presents the estimation of the first six modal parameters (operational frequencies and modes shapes) obtained using the PP method after comparing the results from the three mentioned methods.

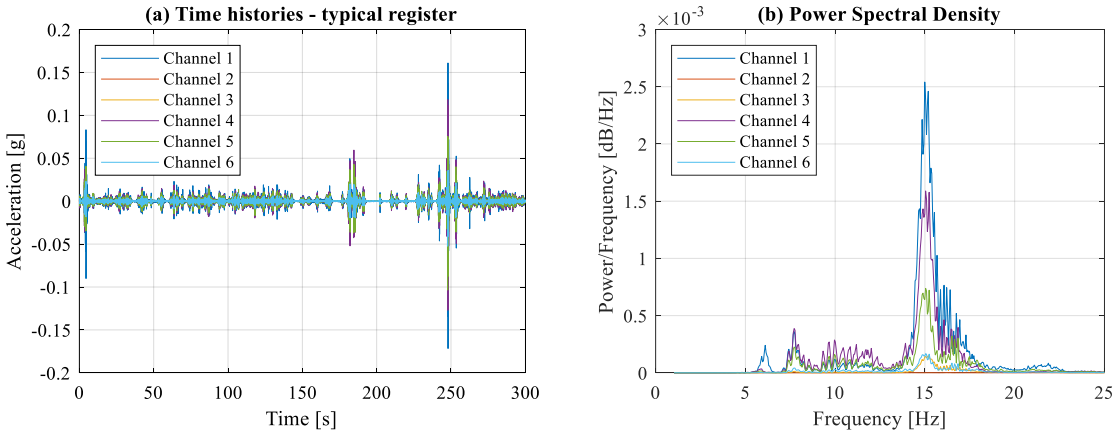

Fig. 6—Signals in the (a) time and (b) frequency domains.

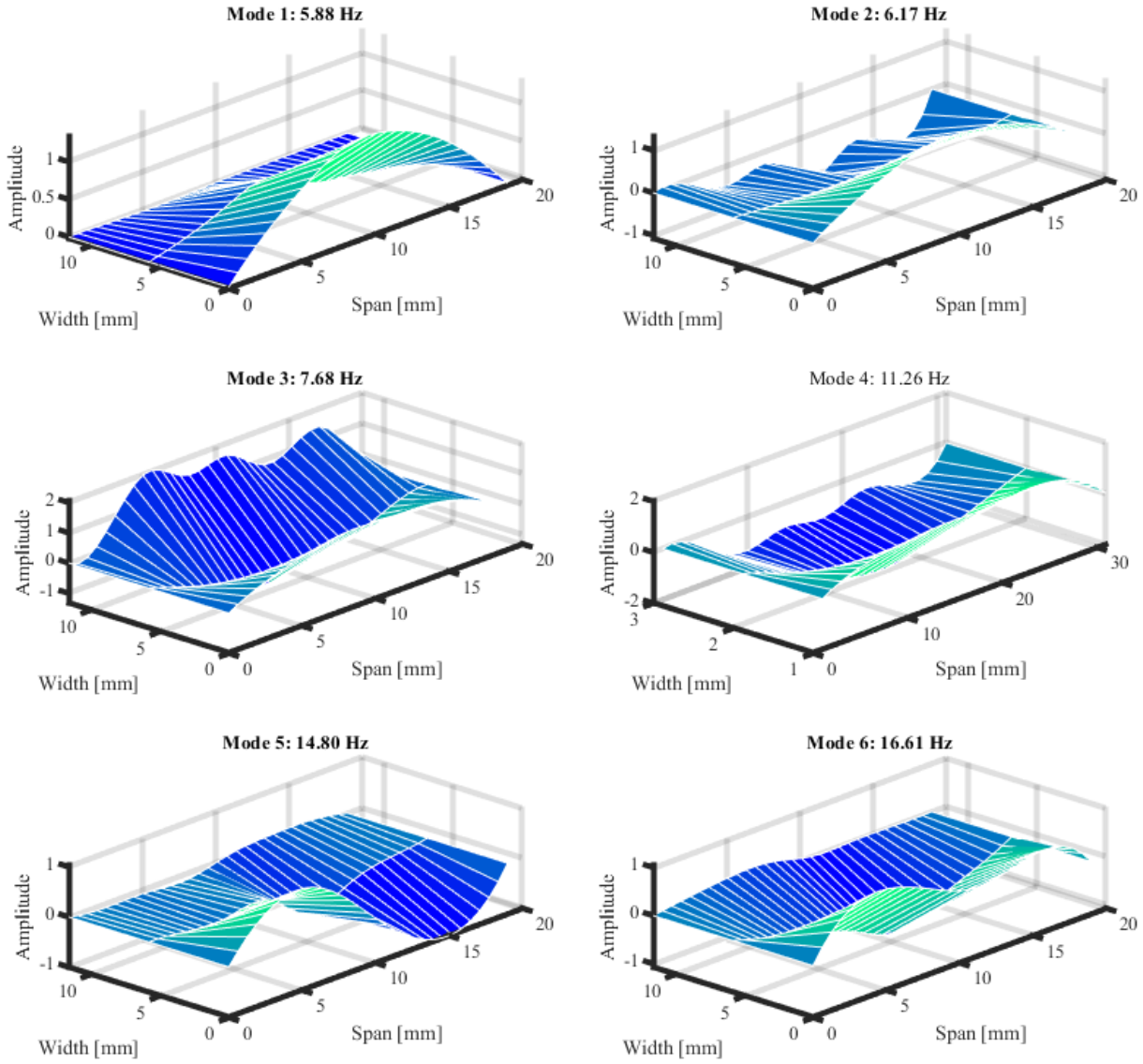

Fig. 7—Estimated modal parameters (operational frequencies and modes shapes) for modes 1 – 6. [1 mm = 0.0394 in.]

Preparation of load test

In the load testing process (diagnostic load tests or proof load tests), three stages are identified: preparation, execution, and analysis of results. In this research, the preparation stage consisted of defining the critical truck location that produces the highest bending moment in the girders and proposing an instrumentation plan based on these positions of interest [26]. Based on the visual inspection of the bridge (Fig. 3), shear was not an expected failure mechanism in the structure.

The analysis of critical position was made using a single design truck from CCP-95 (Fig. 4) and an initial SAP2000 finite element model. The decision to use a single truck in the simulation was because a single truck would be used in the load test due to budget restrictions and execution permits. Based on the SAP2000 model, influence areas (IA) of each girder were constructed to verify the critical position of the truck. For all simulated scenarios, the longitudinal stress in the middle of the section of the bottom flange of the girders was acquired. At these points, the greatest strains occur according to the analysis carried out with the initial model. The IAs were constructed by varying the transverse position (TP) of the truck on the bridge. Vehicle TP is defined as the distance from the curb to the outermost face of the left tire. A series of TPs from 0.7 m to 7.31 m were defined, with 18 equally spaced variations. In each TP, a

simulation was carried out with the C 40-95 design truck traveling at 1 m/s (2.24 mph) and the influence line per unit load was built.

For illustrative purposes, the IAs for girders 1, 4 and 7 are shown in Fig. 8. One truck located in the middle of the span over girders 1, 4 and 7 generated the maximum bending moments in these girders. Thus, these positions were used during the load test. Finally, based on the results of the prestressing force estimate, visual inspection, and as a conservative criterion, a diagnostic load test was performed with a truck weighing less than the design truck.

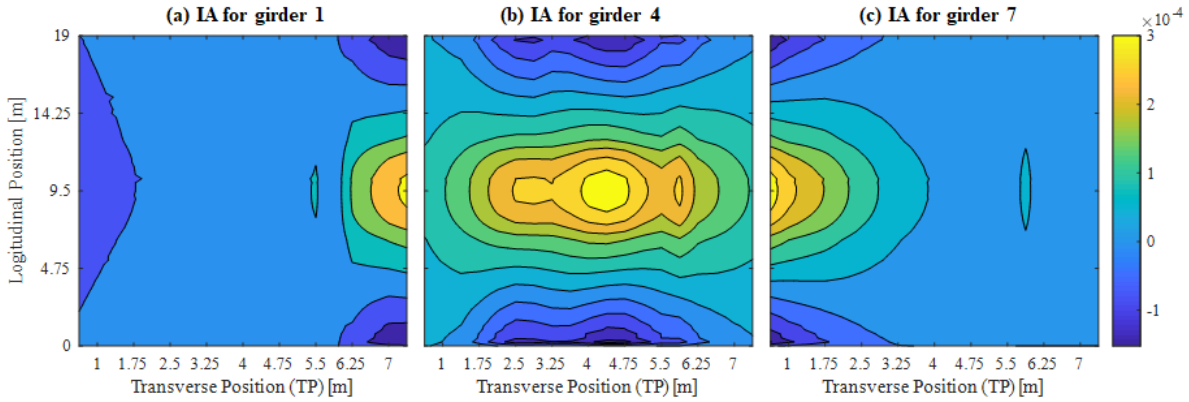

Fig. 8—Influence areas IA for girders 1, 4 and 7. Units in 1/N [1 kN = 0.2248 kip; 1 mm = 0.0394 in.]

Fig. 9 shows the instrumentation plan. Ten strain gauge sensors were installed on the bridge. All strain gages were installed at midspan of the girders. The majority of the strain gauges were placed at the bottom of the cross-section (see Fig. 9), whereas on girders 2, 4, and 7, strain gauges were placed at different heights to derive the strain profile over the height. All strain gages were equipped with their respective compensation gauge. The strain gauges have a length of 90 mm (3.55 in.) and strain limit of 2% and are suitable for measurements on concrete where an inhomogeneous strain field is expected. An adequately averaged strain value is obtained when the length of measuring gauge is at least four times, or preferably five times, the largest aggregate core size[27]. Based on the CCP-95 specifications, the maximum aggregate size of the concrete in the girders was assumed to be 19 mm (0.75 in.).

Since a limited number of ten gauges could be installed given the available instrumentation equipment, the criteria for installation were as follows: (i) one interior girder and one exterior girder should have strain gauges distributed over the height, (ii) at least one interior girder should have three strain gauges for checking experimentally the presence of composite behavior, and (iii) the most deteriorated girder should have strain gauges distributed over its height too. Based on these criteria, one girder would be left without instrumentation. Beam 6 was not instrumented since there may be additional effects on the exterior girders that are not seen on the interior girders.

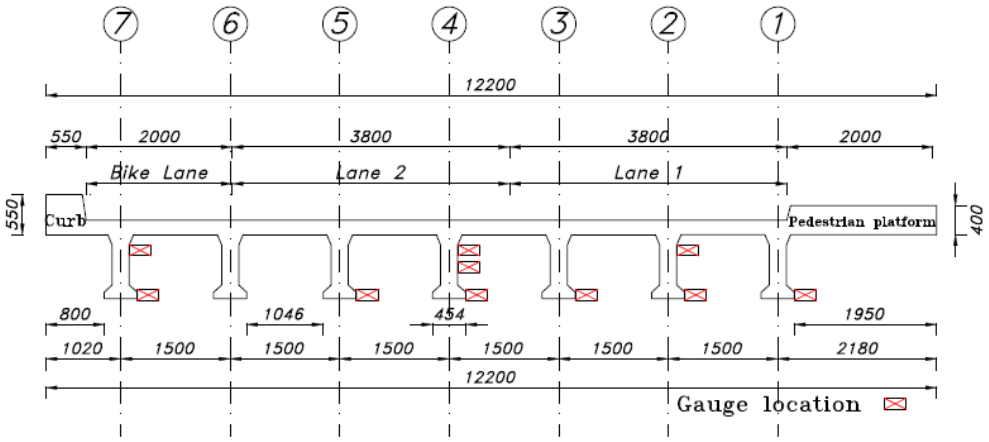

Fig. 9—Strain gauge instrumentation plan. Dimensions in mm [1 mm = 0.0394 in.]

The truck loading test plan consisted of applying static load with one truck at three different positions as shown in Fig. 10. In the load test, the truck was stopped and remained at midspan of each run (Lane 1-L1: truck on Lane 1, right wheel line on girder 1; Lane 2-L2: truck on Lane 2, left wheel line on girder 6; Lanes 1 and 2 -L12: truck between Lanes 1 and 2, truck axis between girders 3 and 4). The position on girder 7 was discarded because the bike lane could not be invaded. The characteristics of the loaded dump truck used for the load test are shown in Table 3, where the total weight of the truck corresponds to 54% of the load of the design truck. This weight guarantees measurable strain responses in the girders[12] and does not generate additional damage to these elements.

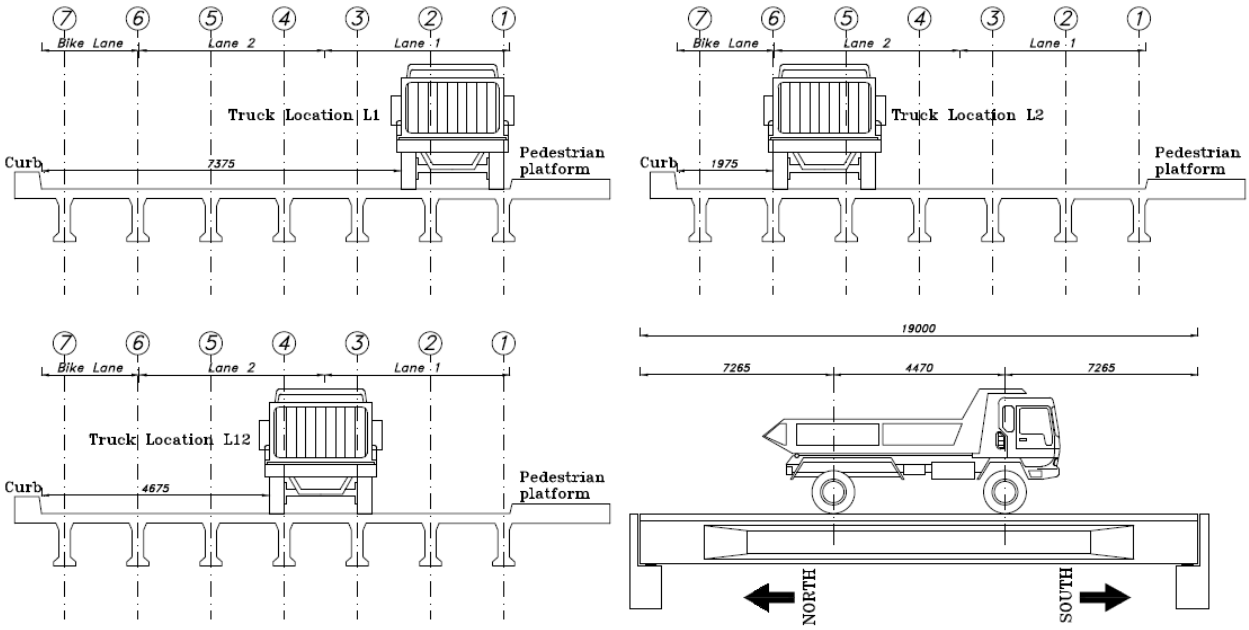

Fig. 10—Static loading plan. Dimensions in mm [1 mm = 0.0394 in]

Table 3—Weights and dimensions of the dump truck.

Parameter	Units	Value
Axle separation	m (ft)	4.47 (14.7)
Wheel line separation	m (ft)	1.85 (6.1)
Total weight	kN (kip)	173.9 (39)
Front axle weight	kN (kip)	40.2 (9)
Rear axle weight	kN (kip)	133.7 (30)

Execution of load test

The execution of the load test and results are shown in Fig. 11. The strain versus time plots show how the strain readings return back to their initial values after unloading the bridge. This behavior indicates that the structure remains in its original state (no additional damage was generated with the load tests). The results from the static load L1 show a higher level of strain on girder 1 as compared with the other elements. A first hypothesis for this outcome is that the level of deterioration in girder 2 resulted in a stiffness reduction, so that relatively more load is redistributed to girder 1, which, in turn, results in the higher strain reading. Even in the load test L12, in which the truck was closer to girder 2, the strain in girder 1 is higher than in girder 2. The peak in the strain data from girder 1 during static load test L1 was due to a sudden movement of the truck (abrupt braking). This value is discarded for the analysis as well as the peaks outside the duration of test L12 due to normal traffic flow before and after testing.

Fig. 12 summarizes the strain results for the three load tests. With this information, the finite element models were updated, and the experimental DFs were calculated.

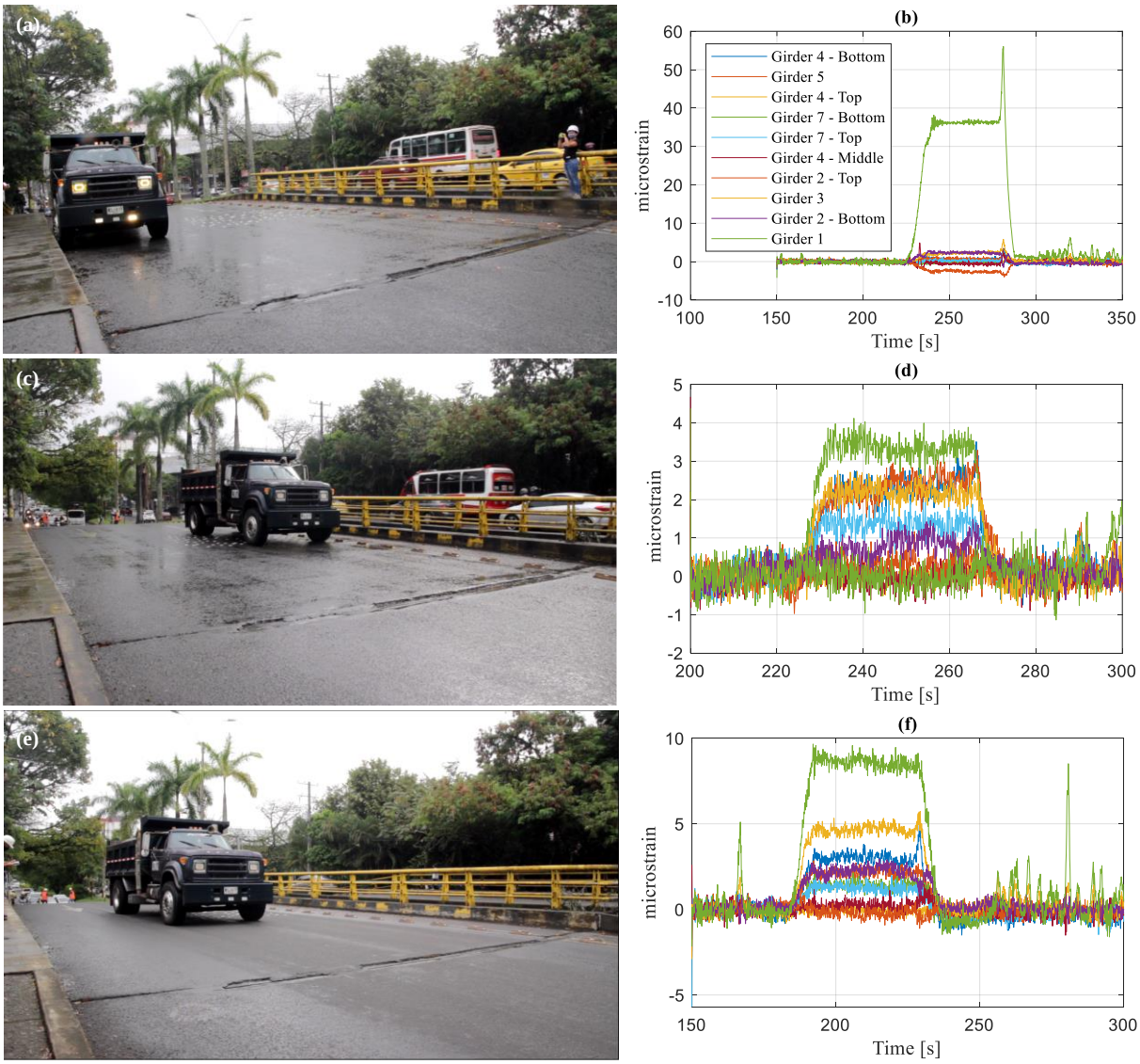

Fig. 11—Load test execution and results: (a) truck location L1; (b) strain static load test L1; (c) truck location L2; (d) strain static load test L2; (e) truck location L12; (f) strain static load test L12.

Fig. 12—Static test transverse strain profile. [1 m = 39.4 in.]

FINITE ELEMENT MODEL UPDATING

The finite element model (FEM) of the bridge was constructed in SAP2000 v18[28] as shown in Fig. 13; the girders, diaphragms and slab were modeled as 2D shell elements and analyzed with thin-plate (Kirchhoff) theory. Tendon elements were utilized to account for the effects of prestress in the analyses. The deck and girder (including diaphragms) concrete strengths were assumed to be 28 MPa (4061 psi) and 35 MPa (5076 psi), respectively. The resulting FEM has 5091 nodes and a maximum mesh size of 100 mm (3.94 in.).

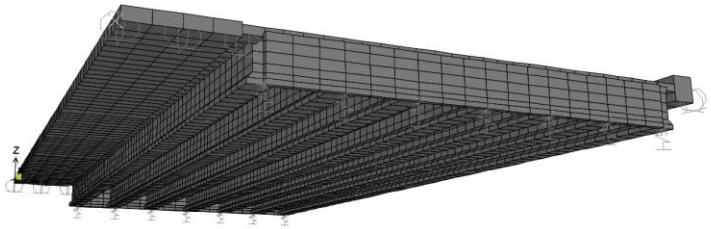

Fig. 13—Finite element model in SAP2000

The model of the bridge was updated sequentially including more field data to improve the agreement with the experimental response as follows:

- update with the OMA results, and
- update with the load tests results.

The initial model was updated with the experimental modal information. Based on the survey, it was observed that the diaphragms at third-span were geometrically inadequate to contribute to the structural system (Fig. 14). Therefore, they were removed from the model and assigned as load (mass) only. Also, based on the OMA results, nonstructural elements, such as the curb and the pedestrian platform, contribute to the stiffness of the structure. By including these elements, the FEM changes drastically, and the frequencies and modal coordinates show a better agreement with their experimental pairs. Other properties, such as the vertical stiffness of the bearings, modulus of elasticity of the concrete in the girders and in the deck were updated (Table 4) in an automatic way by minimizing the following objective function (F) (Eqn. 9):

$$F = \sum_{i=1}^{5} \left| \frac{fn_{ei} - fn_{ai}}{fn_{ei}} \right| + \sum_{i=1}^{5} 1 - \frac{\left(\varphi_{ai}^{T} \varphi_{ei}\right)^{2}}{\varphi_{ai}^{T} \varphi_{ai} \varphi_{ei}^{T} \varphi_{ei}} \tag{9}$$

where fn_{ei} and fn_{ai} are the i-th experimental and analytical frequency, respectively, and φ_{ei} and φ_{ai} are the i-th experimental and analytical modes, respectively, the superscript T indicates the transpose of the modal shape.

Table 4—Initial and updated values for the OMA update.

Variable	Units	Initial value	Final value
Elastic modulus of girders	MPa (ksi)	28390.0 (4177.6)	30195.3 (4379.4)
Elastic modulus of deck	MPa (ksi)	21988.4 (3189.2)	23168.0 (3360.2)
Vertical stiffness girder 1. North – South	kN/mm (kip/in.)	92.4 (527.6) – 92.4 (527.6)	133.1 (760.0) – 133.1 (760.0)
Vertical stiffness girder 2. North – South	kN/mm (kip/in.)	92.4 (527.6) – 92.4 (527.6)	66.56 (380.1) – 133.1 (760.0)
Vertical stiffness girder 3. North – South	kN/mm (kip/in.)	92.4 (527.6) – 92.4 (527.6)	66.56 (380.1) – 66.56 (380.1)
Vertical stiffness girder 4. North – South	kN/mm (kip/in.)	92.4 (527.6) – 92.4 (527.6)	66.56 (380.1) – 66.56 (380.1)
Vertical stiffness girder 5. North – South	kN/mm (kip/in.)	92.4 (527.6) – 92.4 (527.6)	66.56 (380.1) – 66.56 (380.1)
Vertical stiffness girder 6. North – South	kN/mm (kip/in.)	92.4 (527.6) – 92.4 (527.6)	66.56 (380.1) – 66.56 (380.1)
Vertical stiffness girder 7. North – South	kN/mm (kip/in.)	92.4 (527.6) – 92.4 (527.6)	72.59 (414.5) – 66.56 (380.1)

The indicators of the result of the update are presented in Table 5, where the Modal Assurance Criterion (MAC) is used for statistical data analysis as a quality indicator of the experimentally found mode shapes (last quotient in Eqn. 9). MAC is limited between zero when the mode shapes are completely unrelated and one, when they are completely correlated measuring the degree of consistency or linearity of the mode shapes[29].

Fig. 14— Diaphragms at first third-span: (a) general view; (b) diaphragms between girders 1 and 4.

Table 5—Indicators of the OMA update.

Mode	Frequency difference [%]	MAC
1	4.7	0.97
2	1.2	0.86
3	1.8	0.92
4	1.1	0.84
5	18.0	0.89
Mean	5.4	0.89

The OMA updated model was manually calibrated by using an objective error function to assess the closeness of the strain responses in the model to the bridge sensors measurements during the static load test. The mean absolute percent error (*ME*) was used as objective function[8] (Eqn. 10):

$$ME = \frac{1}{n}\sum_{i=1}^{n}\frac{|M_i - P_i|}{|M_i|} \quad (10)$$

where M_i is the measured value from testing for sensor i; P_i is the predicted value from the FEM at sensor i's location; and n is the number of sensors. The parameter for variation was the effective stiffness in the locations of the cracks for each girder, most located in the middle third of the span. To obtain the effective stiffness values from the FEM, different moment-curvature diagrams (Fig. 14) were constructed based on the simple and composite section, the calculated effective prestress force F_e, and the material properties from the Colombian specifications.

Results in Fig. 15 indicate that the simple section exceeds its linear behavior for the total design load ($MT = M_g + M_{ad} + M_{truck\ load}$ where M_g is self-weight moment of girder, M_{ad} is the moment from superimposed dead load and $M_{truck\ load}$ is the live load moment due to the C32-95 or C40-95 design truck), while the composite section remains within its linear range for the full design load, including the C40-95 truck. This indicates that the loss in prestress force could be larger than originally estimated (15%). Thus, the effective stiffness was changed as a percentage of the gross section until a minimum value of *ME* = 0.33 was reached. For each girder, a cracking section was modeled at crack positions obtained from the visual inspection. the moment of inertia at these locations was changed manually from 100% to 30% of the gross moment of inertia of the composite section (Fig. 16). The calibration with the static load test data was performed only for the L12 test. The other results were compared with the updated model to validate the calibration.

Fig. 17 summarizes the cross-sectional strain profile results for the load tests (*LT*) and different updated models: basic model without calibration (*SAP/BASIC*), the model with OMA calibration (*SAP/OMA*), and the model with the OMA update and the load test results calibration (*SAP/OMA+LT).* The results show that the basic model (*SAP/BASIC*) does not represent a good approximation of the experimental results. The first approximation is based on material assumptions and the geometric survey results, without including boundary conditions that simulate neoprene bearings and without excluding diaphragm stiffness. The updated model (*SAP/OMA)* contains the changes showed in Table 4 and the exclusion of the stiffness of the diaphragms. Although this model captures the overall behavior of the structure,

it does not show a good approximation with the experimental strain data. The last updating *(SAP/OMA+LT)* includes the damage at the element level, this input in the FEM has the largest effect on the model outcome to have it more in line with the experimental results of the load tests.

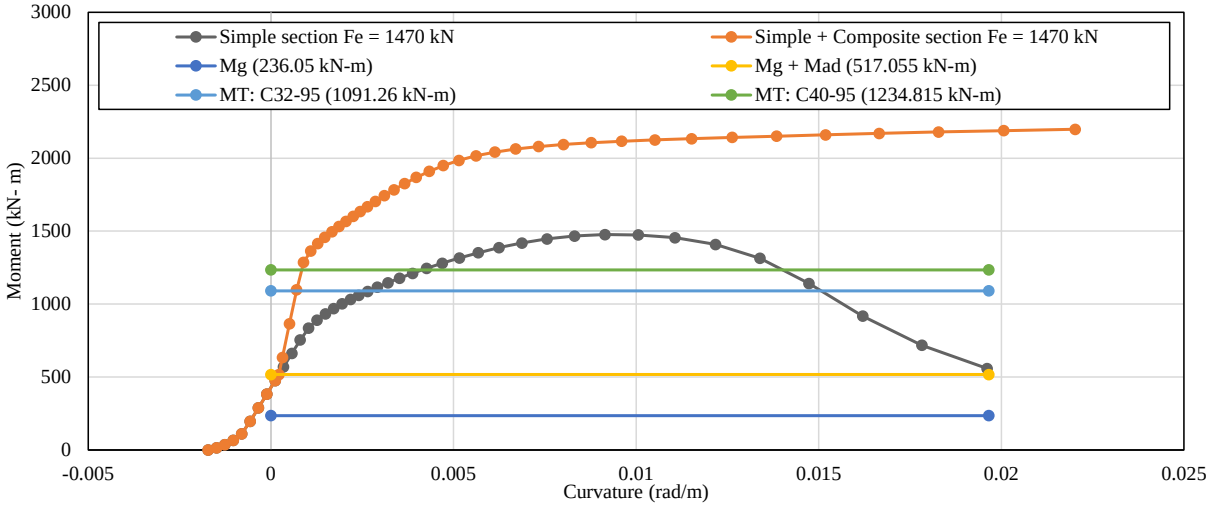

Fig. 15—Moment-curvature diagrams. [1 kN = 0.2248 kip; 1 kN-m = 0.06852 kip-ft]

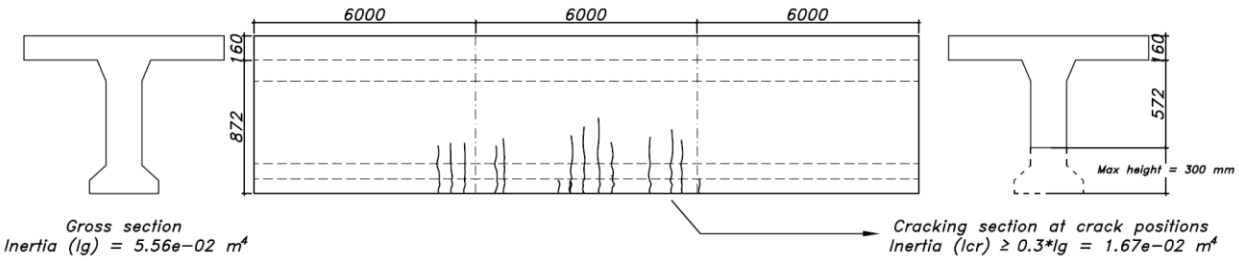

Fig. 16—Girder gross and effective sections [1 m = 39.4 in.]

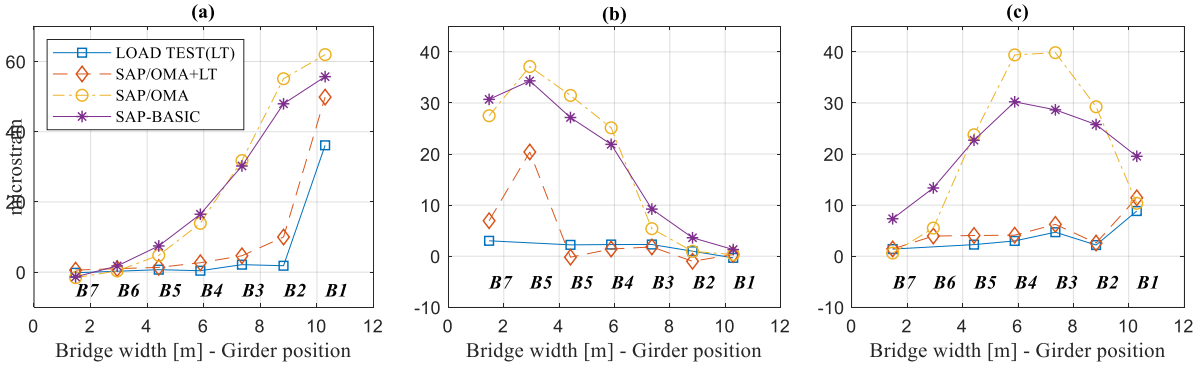

Fig. 17—Strain profiles of updated models: (a) Test L1; (b) Test L2; (c) Test L12. [1 m = 39.4 in.]

LOAD DISTRIBUTION FACTORS

Load distribution factors were calculated with Eqn. 7 using the strain results from the updated models. The LDFs were compared to the load distribution factors calculated using the Colombian (AASHTO) specifications. Fig. 17 shows the LDF for the different levels of calibration and those obtained from AASHTO Standard specification (AASHTO 1992, 1996, 2002 and CCP-95) and AASHTO LRFD Specifications (AASHTO 2014, 2020 and CCP-14). Results in Fig. 18 indicate that the LDFs do not change significantly if the modal information is used to update the basic model, no matter the truck position. However, when the girder deterioration is included in the *SAP/OMA+LT* model, the LDFs

change drastically, and the position of the truck becomes important. AASHTO estimations were not in line with initial FEM results; they even overestimated the values obtained from basic FEM (*SAP-BASIC*) and updated FEM with OMA results (*SAP/OMA*). Fig. 18 (a) and Fig. 18 (b) show that the LDFs of girder 1 and girder 6 are higher than the AASTHO values when the FEM is updated with load test data (*SAP/OMA+LT*). Note that girder 6 was not instrumented and that the FEM calibration with the static load test data was performed only for the L12 test.

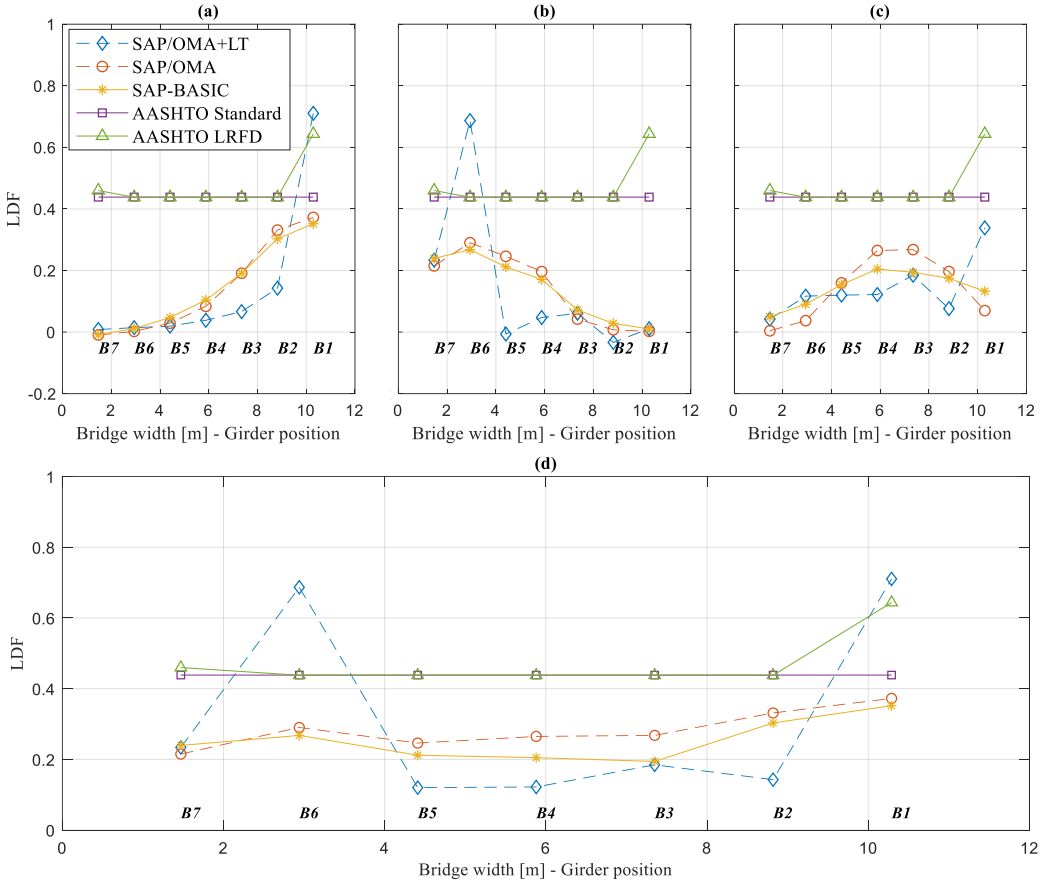

Fig. 18—LDF factors: (a) Truck location L1, (b) Truck Location L2, (c) Truck location L12 and (d) Maximum values for each girder from (a) to (c). [1 m = 39.4 in.]

DISCUSSION

The modeling and experimental analysis of the bridge over the Lili River revealed valuable information regarding the use of field testing and finite model updating to represent the actual behavior of a prestressed concrete girder bridge with deterioration.

The dynamic information obtained through experimental acceleration records is often used to validate the assumptions in finite element models such as boundary conditions, material properties, and the additional stiffness of elements that are not considered in the design[11]. In this research, the modal information is used to adjust the assumed modulus of elasticity and the stiffness of beams bearings. The initial values of elastic modules of the girders and the deck increased 6.4% and 5.4%, respectively. The initial value of the stiffness of beams bearings was modified in a range of 72% and 144%. The OMA results also show the need to add the stiffness provided by the curb and the sidewalk. This addition of nonstructural elements is in line with the work by Barker et al[30] where elements like curbs and railings contribute additional system stiffness. It is recommended to use modal information as complementary information and not as unique experimental information. It is evident that with the results presented from the static tests in this research that the modal information is not sufficient to represent the behavior of the structure.

The simple and composite section assumptions, together with the estimation of the prestressing force, gave an additional estimate of the behavior of the bridge, these steps were necessary because the bridge's plans were missing.

The results showed that the structure is not designed for the heaviest design truck (C40-95), since the regulations at that time allowed the use of the lighter truck (C32-95) based on the function of the roadway where the bridge is located. Based on the level of bridge deterioration, the analysis was complemented with moment-curvature diagrams of the simple and composite girder section. The estimated force, including losses, and the behavior as a composite section indicated that damage in the girders is not expected under service loads since the allowed design tensile stress at service (Table 1) is lower than the theoretical value of concrete tensile cracking stress. However, the visual inspections shows that the girders have severe levels of deterioration. The damage found during the visual inspection was in the middle third of the span and the cracks are vertical and parallel to each other, which indicates flexural distress. The possible reasons are: (i) that the losses in the prestressing forces could be greater than those estimated; (ii) the poor execution of the diaphragms so that the effect of internal supports that these elements provide is removed and the girder is loaded over its full span or, (iii) truck overloads. Estimating the working prestressing in the girders would require additional testing, such as microcore drilling or even testing to induce cracking [31]. Although rating the bridge was not part of the objectives of the research, determining the load rating and possible posting limits is important given the deterioration of the primary load-carrying elements. These elements should not have suffered structural damage.

The instrumentation used in this research was limited compared to other investigations[2,10,11]. However, the strain readings were valuable and sufficient to obtain the actual distribution of live loads in the bridge. The lack of instrumentation on girder 6 may be considered a gap in the experimental information. Nevertheless, the use of a FEM that includes the deterioration of the existing elements helps to predict the strains of this element. Moreover, the number of trucks used during the load tests was less than what is commonly used (2 or more), this was due to budget constraints. Although more trucks could have been useful (i.e., to find the effect of having multiple lanes loaded at the same time) the load tests were designed to cause measurable structural responses on the bridge girders except for girder 7 as driving the dump truck on the bike lane was not possible.

The distribution factors determined based on the experimental strain profiles and the updated model give an indication of the actual behavior of the bridge including its deterioration level. A better rating of the bridge can be calculated by using the LDFs obtained from the updated model using all the experimental information. Besides, the AASHTO LDFs are not in line with FEM results (basic or updated models). In the case of girders B1 and B6, the distribution factors of the deteriorated bridge exceed the values determined by the AASHTO specifications.

In the updated models, the effect of the modulus of elasticity and the vertical stiffness of the bearings was important in adjusting the overall behavior of the structure but did not have much influence on the local behavior of the elements. On the contrary, the modification of the stiffness of the elements by changing the effective inertia in the cracked areas of the beams was very influential. This change allowed the FEM to reach an approach to the experimental strains obtained during the load tests.

CONCLUSIONS

The results of the modeling and analysis of a prestressed girder bridge before and after a diagnostic load test led to the following conclusions:

- The results based on the properties of materials and composite behavior of the typical section, and Magnel diagrams indicate that the structure was designed for the light truck from the Colombia Code (C32-95).
- Since there are no construction plans or design details, information like the geometric survey with the visual inspection, the experimental modal properties based on acceleration records, and the experimental strains from the diagnostic load test allowed know the state of the bridge and its actual performance. This is very important for future analysis of the structure to prioritize maintenance, repair, or reinforcement plans.
- The modal information obtained from OMA and used to update the finite element model was insufficient to represent the experimental strains in the load tests. For the finite element model to better correspond with the field measurements, it was necessary to include the deterioration observed in the visual inspection. This was achieved by modifying the effective stiffness of the most deteriorated girders and comparing the behavior with data from one of the static tests to obtain representative results.
- The results show that the AASHTO recommendations overestimate the LDF when compared to those from the FEM that did not include girder deterioration. Inclusion of girder deterioration in the model changed the LDFs, and AASHTO estimations were not in line with the experimental results. As such, for cases of bridges with severe levels of deterioration, it is recommended to use field data to estimate the distribution factors.

ACKNOWLEDGEMENTS

This study was supported by the Universidad del Valle and the Ministerio de Ciencia Tecnología e Innovación – Minciencias from Colombia. The first author would like to acknowledge the Colombian Doctoral Formation Scholarship No. 647/2015 provided by Colciencias. The second author would like to acknowledge the Colombian Doctoral Formation Scholarship No. 727/2015 provided by Colciencias. Special thanks to the undergraduate students Mauricio Marín and Sebastián Vélez from the Universidad del Valle, and civil engineer Emilia Andrade from the Universidad San Francisco de Quito who worked on this research.

REFERENCES

1. A. Bagheri, M. Alipour, O. E. Ozbulut, D. K. Harris, "A nondestructive method for load rating of bridges without structural properties and plans," *Eng. Struct.* 171, 545–556 (2018).
2. C. V. Aguilar, D. V. Jauregui, B. D. Weldon, C. M. Newtson, "Rating of Prestressed Concrete Adjacent Beam Bridges without Plans," Spec. Publ. 323, 5.1-5.20 (2018).
3. F. Biondini and D. M. Frangopol, "Life-Cycle Performance of Deteriorating Structural Systems under Uncertainty: Review," *J. Struct. Eng.* 142(9), F4016001 (2016).
4. E. O. L. Lantsoght, C. van der Veen, A. de Boer, D. A. Hordijk, "State-of-the-art on load testing of concrete bridges," *Eng. Struct.* 150, 231–241 (2017).
5. American Association of State Highway and Transportation Officials (AASHTO), *The Manual for Bridge Evaluation*, 3rd Edition, Washington, D.C. (2018).
6. American Association of State Highway and Transportation Officials (AASHTO), *AASHTO LRFD Bridge Design Specifications*, 9th Edition, Washington, D.C. (2020).
7. E. O. L. Lantsoght, C. van der Veen, A. de Boer, J. C. Walraven, "Using Eurocodes and Aashto for Assessing Shear in Slab Bridges," *Proceedings of the Institution of Civil Engineers - Bridge Engineering*. 169 (4), 285–297 (2016).
8. American Concrete Institute (ACI), *ACI 342R-16 Report on Flexural Live Load Distribution Methods for Evaluating Existing Bridges*, ACI (2016).
9. E. Ohanian, D. White, and E. S. Bell, "Benefit Analysis of In-Place Load Testing for Bridges," *Transportation Research Board 96th Annual Meeting* (2017).
10. V. Torres, N. Zolghadri, M. Maguire, P. Barr, M. Halling, "Experimental and Analytical Investigation of Live-Load Distribution Factors for Double Tee Bridges," J. *Perform. Constr. Facil.* 33(1), 04018107, American Society of Civil Engineers (2019).
11. C. Dong, S. Bas, M. Debees, N. Alver, F. N. Catbas, "Bridge Load Testing for Identifying Live Load Distribution, Load Rating, Serviceability and Dynamic Response," *Front. Built Environ.*, Frontiers (2020).
12. S. Alampalli, D. M. Frangopol, J. Grimson, D. Kosnik, M. Halling, E. O. L. Lantsoght, J. S. Weidner, D. Y. Yang, Y. E. Zhou, "Primer on Bridge Load Testing," Transportation Research Board (TRB) (2019).
13. A. Halicka, D. A. Hordijk, and E. O. L. Lantsoght, "Rating of Concrete Road Bridges with Static Proof Load Tests," *Spec. Publ. 323*, 3.1-3.16 (2018).
14. Ministerio de Transporte: Instituto Nacional de Vías, *Código Colombiano de Diseño Sísmico de Puentes*, AIS, Bogotá, Colombia (1995).
15. American Association of State Highway and Transportation Officials (AASHTO), *Standard specifications for highway bridges*, 15th Edition, Washington, D.C. (1992).
16. Asociación Colombiana de Ingeniería sísmica - AIS, *Norma Colombiana de Diseño de Puentes CCP 14*, AIS, Bogotá, Colombia (2014).
17. American Association of State Highway and Transportation Officials (AASHTO), *AASHTO LRFD Bridge Design Specifications*, 6th Edition, Washington, D.C. (2012).
18. American Association of State Highway and Transportation Officials (AASHTO), *AASHTO LRFD Bridge Design Specifications*, 7th Edition, Washington, D.C. (2014).
19. M. Arockiasamy and A. Amer, "Load Distribution on Highway Bridges Based on Field Test Data: Phase Two," *WPI 0510668*, Florida Atlantic University, Bocca Raton, FL, p. 213 (1998).
20. M. Araujo, "Slab-on-girder prestressed concrete bridges: linear and nonlinear finite element analysis and experimental load tests," LSU Doctoral Dissertations, Louisiana State University (2009).
21. A. E. Naaman, *Prestressed Concrete Analysis and Design: Fundamentals*, 2nd Edition, Techno Pr 3000, Ann Arbor, Mich (2004).
22. D. J. Ewins, *Modal Testing: Theory, Practice and Application*, 2nd Edition, Research Studies Press ltd. (2000).

638 23. G. H. James III, T. G. Carne, and J. P. Lauffer, "The natural excitation technique (NExT) for modal parameter
639 extraction from operating wind turbines," *NASA STIRecon Tech. Rep. N 93* (1993).
640 24. P. Van Overschee and B. De Moor, *Subspace Identification for Linear Systems*, Springer US, Boston, MA (1996).
641 25. S. Castellanos-Toro, M. Marmolejo, J. Marulanda, A. Cruz, P. Thomson, "Frequencies and damping ratios of
642 bridges through Operational Modal Analysis using smartphones," *Constr. Build. Mater.* 188, 490–504 (2018).
643 26. E. A. Andrade Borges, E. O. L. Lantsoght, S. Castellanos-Toro, J. Marulanda, "Modeling and analysis of a
644 prestressed girder bridge prior to diagnostic load testing," *ACI Av. En Cienc. E Ing*. **unpublished article** (2021).
645 27. K. Hoffmann, An Introduction to Measurement Using Strain Gages, Hottinger Baldwin (1989).
646 28. CSI, "SAP2000 Integrated Software for Structural Analysis and Design," Version 18, Computers and Structures
647 Inc., Berkeley, California.
648 29. M. Pastor, M. Binda, T. Harčarik, "Modal Assurance Criterion," *Procedia Engineering*, 48, 543–548 (2012).
649 30. M. G. Barker, "Quantifying Field-Test Behavior for Rating Steel Girder Bridges," *Journal of Bridge Engineering*.
650 6 (4), 254–261 (2001).
651 31. E. O. L. Lantsoght, G. Zarate, F. Zhang, M.-K. Park, Y. Yang, H. Sliedrecht, "Shear Experiments of Prestressed
652 Concrete Bridge Girders," *ACI Structural Journal*. 118 (3), 117–130 (2021).
653
654

Sebastián Castellanos-Toro is a civil engineering PhD Student and research assistant at Universidad del Valle, Cali, Colombia, and member of Grupo de Investigación en Ingenierías Sísmica, Eólica, Geotécnica y Estructural (G-7). His research interests include structural dynamics, instrumentation and structural monitoring, assessment of existing structures, reliability of structures, among others.

Diana Millán is a civil engineering PhD student and research assistant at Universidad del Valle, Cali, Colombia, and member of Grupo de Investigación en Ingenierías Sísmica, Eólica, Geotécnica y Estructural (G-7) research group. She received her MS in civil engineering from Universidad del Valle, Cali, Colombia, in 2015. Her research interests include structural dynamics, instrumentation and structural monitoring, deterioration models, among others.

Albert R. Ortiz is an associate professor at Universidad del Valle, Cali, Colombia, and member of Grupo de Investigación en Ingenierías Sísmica, Eólica, Geotécnica y Estructural (G-7) research group. He received his MS in civil engineering from Universidad del Valle, Cali, Colombia, in 2011 and his PhD in civil engineering from the University of South Carolina, Columbia, SC, USA, in 2016. His research interests include structural dynamics, instrumentation and structural monitoring, human-structure interaction, reliability of structures, among others.

Johannio Marulanda is a full professor at Universidad del Valle, Cali, Colombia, and member of Grupo de Investigación en Ingenierías Sísmica, Eólica, Geotécnica y Estructural (G-7) research group. He received his MS in civil engineering from Universidad del Valle, Cali, Colombia, in 2006 and his PhD in civil engineering from the University of South Carolina, Columbia, SC, USA, in 2010. His research interests include structural dynamics, experimental dynamics, instrumentation, and structural monitoring, among others.

Peter Thomson is a full professor at Universidad del Valle en Cali, Colombia, and head of Grupo de Investigación en Ingenierías Sísmica, Eólica, Geotécnica y Estructural (G-7) research group. He received his MS and PhD in aerospace engineering and mechanics from University of Minnesota, Minneapolis, MN, USA, in 1994 and 1995, respectively. His research interests include structural dynamics, structural control, structural health monitoring, among others.

ACI member **Eva O. L. Lantsoght** is a Full Professor at Universidad San Francisco de Quito, and an Assistant Professor at the Delft University of Technology. She is the Vice-Chair of ACI 445-0E Torsion, member of ACI 445-0D Shear Databases, ACI 342, Evaluation of Concrete Bridges and Bridge Elements, and ACI-ASCE 445, Shear and Torsion, Secretary of ACI-ASCE 421, Design of Reinforced Concrete Slabs, and an associate member of ACI 437, Strength Evaluation of Existing Concrete Structures.